

A Test of the Reliability of Mathematically Modeling Corrosion

J. Peter Ault, Jr.
Ocean City Research Corporation
Tennessee Avenue and Beach Thorofare
Ocean City, New Jersey USA

John J. Meany, Jr.
Bismarck, Inc.
PO Box 1006
Ocean City, New Jersey USA

Abstract

Engineers increasingly solve corrosion control design problems and analyze corrosion processes using mathematical models, particularly finite element-type models. Often this approach becomes complicated and its basis obscure. A pragmatic corrosion engineer may wonder if such approaches constitute window dressing and image projection rather than a straightforward and understandable engineering approach.

The present paper compares finite element modeling predictions to the results of a controlled laboratory full scale test. The finite element model supposedly predicted the expected life for the anodic alloy tubing where tubing of two different alloys connected with internal flowing seawater. The full scale test results show that the mathematical model didn't consider either the effects of time and environmental variables or pitting corrosion.

The laboratory test results show that neither the measurement of galvanic current nor the mathematical model calculation forms a basis for estimating of the magnitude of the most important type of corrosion of 70/30 CuNi tubing. The laboratory tests identified pitting corrosion as most important. The deepest pit was not immediately adjacent to the Inconel 625 tubing as most mathematical models predict. For the particular tubing configuration tested, turbulence-induced corrosion caused more damage than that relating to the Inconel 625-70/30 CuNi couple. Thus, in-service mismatches between Inconel 625 and 70/30 CuNi tubing may be of more concern about corrosion of the CuNi tubing than galvanic effects.

The laboratory testing results comprised physical examination of specimens exposed to flowing seawater for six months with the continuous monitoring of the more significant environmental variables. The comparison of modeling predictions and actual tubing corrosion places suspicion upon the mathematical model. It appears that the model provides reasonable "order of magnitude" estimation of galvanic current flow. The model neither accurately predicted long term current distribution nor the magnitude of pitting corrosion. This raises a very pertinent question -- "If a mathematical model can't reliably handle simple galvanic corrosion, how reliable are such models when applied to more complex situations?"

Introduction

OCRC obtained a computer program which had been used to calculate the expected galvanic corrosion rate of 70/30 CuNi alloy piping when coupled to Inconel 625 piping. D.J. Astley developed the technical approach that formed the basis for the program. His paper is entitled, "A Method for Calculating the Extent of Galvanic Corrosion and Cathodic Protection in Metal Tubes Assuming Unidirectional Current

Flow," (Corrosion Science Vol. 23, No. 8, pp 801-832, 1983). The technique described by the paper applies Ohm's and Kirchoff's laws to the piping geometry. It assumes: 1) unidirectional current flow down the length of the pipe; 2) the electrode (metal surface) corrosion potential against a standard electrode varies linearly down the pipe in direct proportion to the local current flow; and 3) the decrease in current flow down the pipe is the result of current flow to the tube wall resulting in local polarization. Tube wall polarization behavior is approximated by a linear polarization resistance term. The present report presents the results of limited testing conducted with the objective of validating the model through the comparison of the results of laboratory test results with those of the model.

Experimental Approach

Figure 1 shows the general arrangement of the testing facility. The unfiltered seawater supply fed into the test run through a Monel-body pressure regulator. This comprised the only metallic element in the seawater supply system. Approximately 30 feet of plastic piping intervened between the regulator and the upstream end of the test pipe run. Adjustment of the pressure regulator set point assured a continuous flow through the test pipe at a velocity of approximately 11 fps. A thermowell upstream of the test piping provided for the measurement of flowing seawater temperature.

Figure 2 shows the layout of the test run itself. The run consists of about 16.2 feet of 70/30 CuNi tubing and about 20 feet of Inconel 625 tubing, both with nominal internal diameters of 0.75 inch. The actual measured inside diameter of the 70/30 pipe approximated 0.90 inch; the Inconel 625 approximated 0.85 inch. Figure 2 shows the segment lengths and their arrangement for both alloys.

Figure 3 shows the method followed for joining the tubing segments, the electrical connections and the provision of capillaries for measurement of segment potentials to a reference electrode. The segments were placed on a tight fitting teflon rod, spaced approximately 0.1 inch apart. A thin glass capillary tube was placed between the two segments, perpendicular to the tubing axis surrounded by a 1/4-inch PVC pipe nipple. Two AWG #12 copper wires were soldered at each end of all segments, providing for electrical contact with the segments. A form was placed around the entire assembly which was then filled with Scotchcast resin. This encapsulation prevented seawater leakage and assured electrical isolation between segments.

Shrink sleeves were installed on four inches of each end of the longer segments. Those segments were then joined using plastic tubing couplings. A 1/4-inch PVC coupling was tapped into the sleeve and a valve placed on the end of the nipple. An adapter allowed connection of a small diameter plastic capillary tube to the downstream end of the valve. Cracking of the valve, allowing slow leakage, and inversion of the downstream end of the capillary in a glass beaker allowed for measurement of the potential of the segments to a reference electrode.

Seawater was introduced into the tubing upon completion of its assembly. Adjustment of the pressure regulator provided for a reasonably constant flow rate through the tubing at a flow velocity of about 11 feet per second. All segments were then short circuited to adjacent segments, except for the joint between the 12-inch Inconel 625 segment and the 0.5-inch 70/30 segment. This condition continued for about two weeks, allowing for reasonable stabilization of potentials.

Precision shunt resistors then installed between all adjacent segments allowed for the measurement of current interchange between segments and the calculation of the values of current interchange between the segment and the flowing seawater. Precision digital voltmeters, Fluke Model 805A, provided

instantaneous measurements of these parameters. Continuous monitoring of current interchange between 70/30 CuNi segments and between the 70/30 CuNi 0.5-inch segment and the 12-inch Inconel 625 segment was performed with recording strip charts in the earlier part of the test run. Later, a personal computer (IBM PC) and an analog to digital board monitored the more important environmental variables, including flowing seawater temperature, resistivity, and turbidity. The following sensors/transmitters were used:

Seawater Temperature	Cole Parmer Digisense, Model 2186
Seawater Resistivity	Foxboro 870EC Transmitter Foxboro 871EC Sensor
Turbidity	Turner Model 40 Nephelometer

An Omnidata "Easy Logger" monitored the potentials across the shunt resistors of the 70/30 CuNi segments for the majority of the test run.

Results and Discussion

Physical Inspection

Figure 4 shows the results of the post test physical inspection of the 70/30 CuNi tubing. The plotted data indicates the deepest pit found in each segment of this tubing. The figure does not show the deepest pit on the entire tubing length. One pit, located about 0.125 inch downstream of the seawater inlet to the tubing, nearly penetrated the .0825-inch tubing wall, indicating a pitting rate of about 161 mils per year. Visual inspection suggested that high turbulence intensity caused this pit. The upstream end of the 70/30 tubing did not mate closely with the adjoining pipe section, there being a transition from CuNi pipe to PVC pipe.

The deepest pit in the region nearest the Inconel 625 tubing was located approximately 8.7 inches upstream of the Inconel. This is near the downstream end of the 5-inch segment. No evidence of typical turbulence-related corrosion was evident.

Figure 5 shows a 20X cross section of the internal surface of the segment immediately adjacent to the Inconel 625 tubing. The slight taper on the right end of the section resulted from reaming of the tubing after cutting prior to the test. No gradual reduction of cross section exists as the finite element predictions suggest.

Current and Potential Monitoring

Galvanic current monitoring showed wide variations of current magnitudes and locations of current interchange between the tubing and seawater. Seawater temperature seemed the major factor affecting the galvanic current. Very frequently, however, variations in galvanic current did not relate to any single monitored environmental variable. The maximum corrosive effects of the galvanic current generally occurred within 12 tubing diameters of the point of connection between the two types of tubing. The maximum corrosive current density values did not exceed 10 microamps/cm² (\approx 10 mils/year corrosion). The magnitude of anodic current density, however, varied over a wide range. The location of the maximum anodic current density also varied. During the early part of the testing, maximum anodic current density generally occurred adjacent to the Inconel 625 tubing. Later, however, anodic

current density frequently occurred 4 inches or further from the Inconel 625 interface. As a practical matter, determination of the cumulative effects of anodic current at any location presents formidable data analysis problems.

Figure 6 shows the values of galvanic current between the two alloy pipes immediately after closing the circuit between the two tubing sections. A computer, with a one-second recording interval, recorded the plotted values.

Measurement of the internal resistance between the two tubing types shortly before circuit closure gave a value of 104.4 ohms. Figure 7 shows a potential profile obtained just before circuit closure. With the measured internal resistance and the open circuit potential between the two tubing types of 0.25 volt, the initial galvanic current value, prior to any polarization of either alloy, would be expected to be:

$$I_g = E_{oc}/R_{int} = 0.25/104.4 = 0.0024 \text{ amperes}$$

Figure 6 shows an initial current value of about 390×10^{-6} amperes, a considerably smaller value than that calculated from the internal resistance and open circuit potential. This indicates that polarization reduced the driving potential substantially during the first second after circuit closure. The figure also shows that the galvanic current did not reach a reasonably stable value until an elapsed time of about one hour after circuit closure.

Figure 8 shows the galvanic current together with the more important environmental variables over the first 24 hours after circuit closure. After the first five hours, the galvanic current varied within a relatively narrow limit, as did the environmental variables, except turbidity, which remained at a relatively high level.

Figure 9 shows potential profiles, one measured during the early part of the test period, the other near the end of the test period. The latter values fall in significantly more active ranges.

Figure 10 shows current profiles on the 70/30 CuNi pipe showing characteristics at four different times during the testing period. The average of the three recorded environmental variables follow:

Test Period <u>hours</u>	Temperature <u>degrees C</u>	Resistivity <u>ohm-cm</u>	Turbidity <u>ju</u>
149 to 179	3.0	45.0	7.5
339 to 349	5.8	37.8	10.5
3984 to 4007	25.4	23.4	13.7
4152 to 4174	25.4	23.9	13.7

Note that the values of resistivity shown are those at flowing seawater temperature. Figure 11 shows typical resistivity-temperature relationships for three levels of chlorinity.

Figure 12 shows the density of current interchange between the tubing and the seawater flowing through it. The figure shows averages for the individual segments. The difference between the magnitudes of current densities between the two curves reflects changes that could not be predicted through passive circuit simulations (e.g., simple mathematical models). The higher current densities in the areas from

3.5 and 12.5 inches upstream of the Inconel 625 seem particularly interesting, seemingly correlating with the location of the deepest pits.

Figure 13 shows total galvanic current and seawater temperature over a 20-hour period midway in the test. Visually, a correlation between the two variables seems evident. Regression analysis showed a relationship as:

$$I_g = 163.2 + 9.41 * T$$

The correlation coefficient R^2 was 0.96, indicating a reasonably good correlation.

Figure 14 shows the total galvanic current together with the three recorded environmental variables over about a 24-hour period in the later part of the test. Visual inspection shows no identifiable correlation between the values of any single variable and the value of galvanic current flow. Also note that the above relationship between galvanic current and temperature would predict a current of about $400\mu\text{A}$ for this period -- significantly lower than the actual current.

Equivalent Circuit Simulations

General. Figure 6 and its previous discussion showed that conventional passive dc circuit analysis can only predict that current that will flow in a galvanic cell at the instant of half cell connection. The significant difference between galvanic current calculated from the open circuit potential and the internal resistance between the two half cells suggest that the initial predicted current flow causes activation polarization of one, or both, of the half cells. The longer term reduction of galvanic current, through the first three hours indicates that concentration polarization significantly affects the galvanic current magnitude. This complicates the true galvanic corrosion cell simulation through any type of fixed electrical analog that does not include time-dependent elements.

Evaluation of the applicability of mathematical models to the prediction of galvanic current values and the distribution of the alloy/electrolyte interchange of the current must first consider the nature of the alloy of concern. The 70/30 copper-nickel alloy typically corrodes in a pitting mode when exposed to relatively slow moving seawater. Many studies conducted by OCRC show that the deepest pits of 70/30 CuNi tubing exhibit an extreme value probability distribution. This means that the greater the length of tubing the deeper the deepest pit will be. A recent OCRC study, conducted under the same conditions as the galvanic corrosion study reported here, showed that a pit whose depth is 15 mils would be expected to be found if 1500 feet of 70/30 CuNi tubing of the same diameter was exposed. Since the length of tubing involved in the present test was only about 16 feet, the probability of finding a pit representing a pitting rate of 15 mils per year would be very unlikely. The location of such a pit near the point of connection to the Inconel 625 would be even more unlikely. It seems reasonable, therefore, to conclude that the galvanic current stimulated the deepest pit near the galvanic couple.

Present mathematical models predict corrosion (anodic) current densities. No studies to date validate any rigorous relationship between pitting corrosion depth and average anodic current density, particularly regarding an alloy with corrosion characteristics similar to those of 70/30 CuNi in flowing seawater. In addition, such models can not predict total corrosion over any period other than that immediately after the assumed polarization characteristics whose values the model uses. The models do not consider the time-dependent characteristics of polarization. The previous discussion illustrated rapid changes in polarization characteristics and extreme variability of environmental conditions that influence the

magnitude of galvanic current. In addition, the discussion showed that, at times, changes in the any individual environmental condition did not correlate with changes in galvanic current values. The mathematical models can predict the general magnitude of expected galvanic current. The model can suggest the degree of probability that the galvanic current will be of sufficient magnitude to affect the corrosion of the anodic half cell; prediction of pitting rates, however, falls beyond the scope of such models. Furthermore, less complex mathematical methods can yield the same general results.

The presently reported testing could not include the determination of any electrochemical characteristics whose determination required impressing significant current between the seawater and the pipe surface. Such action would have disturbed the naturally occurring corrosion phenomenon and invalidated the key element of the program, the physical measurement of the extent of corrosion after completion of the test. Fortunately, data is available from a similar test program previously conducted by OCRC using 70/30 CuNi tubing and flowing seawater. This program included periodic determination of polarization characteristics of the tubing.

Figure 15 shows the results of a determination of the anodic polarization characteristics of the 70/30 CuNi tubing after about 8 months exposure to seawater flowing at about 7 feet per second. The data, plotted in the conventional manner, has a log X-axis.

Figure 16 shows the same data plotted with a linear X-axis. Refer now to figure 9 which shows the tube potentials after two intervals of exposure to flowing seawater. The 288-hour curve shows that the 70/30 nearest the Inconel polarized to an active potential of about -0.08 volt. Now refer to figure 16 which shows that the 70/30, in reaching this potential, passes through different potential/current density relationships. Simplifying this situation, we can strike two straight lines through the curves. The first line, from the zero current density point to about 10 microamps/cm², exhibits a slope of about 1250 ohm-cm². The second slope, using the portion of the data above about 20 microamps/cm², gives a slope of about 13,000 ohm-cm². This would be the expected polarization resistance for those 70/30 CuNi areas closer than about 10 inches to the Inconel.

Now consider the polarization of that portion of the 70/30 tube more than about 10 inches upstream of the Inconel. This area polarized only to about -0.16 volt. This polarization would be in the 1250 ohm-cm² range only, as would that portion of the tube further from the Inconel. Any mathematical simulation that does not consider these differences could not yield accurate data.

Figure 17 shows the changes in polarization resistance throughout the course of the test run from which figures 15 and 16 were derived. A model that does not consider such changes could not yield accurate long-term results.

Another factor that must be considered is the validity of the substitution of passive resistors for the active voltages that exist in the real-life galvanic cell. Most mathematical simulations consider only the initial open circuit potential between the two half cells. They may use the initial half cell potentials to a reference electrode; the galvanic potential between the half cells being the difference between these two potentials. This presents another problem, since the formation of long-duration oxidation or reduction films inherently change the initially assumed open circuit potentials. This is evident in figure 9.

Mathematical Models

Computer Model Analysis. The computer program described in the *Introduction* was run using data gathered in the current effort. The open circuit potential difference was obtained from figure 6 -- about 0.25 volt. The tube dimensions are those actually tested. The polarization resistance value for the Inconel 625 was a commonly accepted value of 520,000 ohm-cm². The polarization resistance values for the 70/30 CuNi were obtained from the previous OCRC testing. Referring again to figure 16, the "average" polarization resistance for the 70/30 CuNi when the couple is under complete anodic control -- worst case for total current -- is about 4,200 ohm-cm². The least attenuation would occur in the situation where the 70/30 CuNi exhibits its highest polarization resistance; for this situation a value of 15,000 ohm-cm² was used for the analysis.

The results of the program runs for each condition were similar -- the results are controlled primarily by the high polarization resistance of the Inconel. In both cases the total predicted current was about 300 μ A which corresponds well with the initial measured currents in the range of 390 μ A. However, as discussed, this current rapidly decreased to about 75 μ A -- about 25% of that predicted. Using an arbitrary "effect" of less than 0.5 mpy as the extent of an effect of the galvanic couple, the models suggest that most of the current will attenuate within 8 to 10 inches. This is relatively good agreement with the observations in the actual test. The predicted galvanic corrosion rates do not agree with those measured. The prediction suggests that the corrosion will attenuate from the couple -- a phenomenon not observed. The maximum corrosion, in the form of pitting, occurred 8.7 inches downstream of the couple.

Tee-Section Analysis. An alternative method, mathematically more simple, for estimating the galvanic corrosion would be a Tee-section attenuation analysis, as shown in figure 18. Assume the length of each section as 10 centimeters. The resistance of the seawater path down tube would be, with a seawater resistivity of 25 ohm-cm, 60 ohms for each section. This would be the value of R_1 in figure 18. R_2 would be the interfacial ohmic resistance. Empirical considerations indicate an assumption of about 70 ohm-cm² would be reasonable for this value. R_3 would be the polarization resistance -- and values of 4,200 to 15,000 ohm-cm² can be used as before. Given the surface area of each segment, 4.1 cm², the complete interfacial resistance would be about 1040 to 3675 ohms. Since our test loop was about 170 inches long, we can assume 43 repetitive test sections of 10 cm each.

Figure 19 shows the attenuation of galvanic current based upon the two polarization resistance values discussed above. Obviously, the higher the assumed polarization resistance, the lesser the attenuation of galvanic current. If the likelihood exists that the galvanic current will accelerate the corrosion pitting rate, then the two curves suggest that, at the worst, one might be concerned about the region in which perhaps the first 50% of the galvanic current interchanges from alloy to seawater. With the larger polarization resistance, this would be the first 20 inches (20 pipe diameters) from the couple. For the lower polarization resistance this would be the first 18 inches -- no major difference between the two values, from a pragmatic standpoint. This agrees well with the measured values.

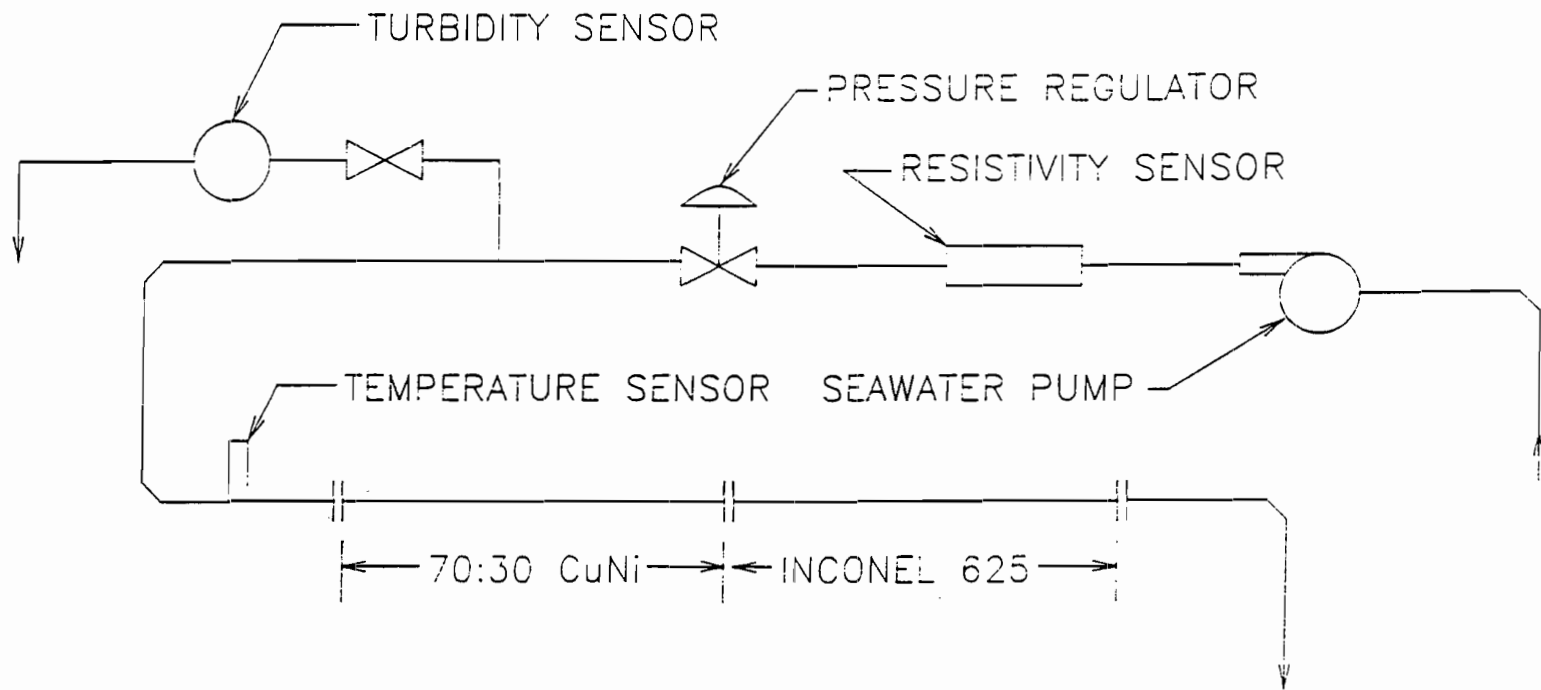
The next important factor focuses on a simple method for determination of a threshold value of total galvanic current that might be a concern as a corrosion accelerating factor on the anodic half cell (70/30 CuNi). The derivation of the actual critical galvanic current value falls beyond the scope of the present study. The polarization resistances of the two alloys of concern differ substantially. 520,000 ohm-cm² represents an accepted value for the Inconel alloy. Figure 20 shows the calculated input resistance value for 1-inch OD Inconel pipe, as a function of pipe length, based upon this polarization resistance value.

The curve derived from resistances calculated for four different lengths of Inconel 625 tubing, using classical mesh network calculations. Obviously, a very short length of Inconel tubing would polarize rapidly if connected to a rather long length of 70/30 tubing. The Inconel's polarization would keep the galvanic current flow to a low value with insignificant corrosion effects.

Using a similar technique to calculate the input resistance of the 70/30 CuNi section (i.e., 16.2 feet in length) used in the current test determines that the input resistance would range from 388 to 472 ohms for polarization resistance values from 4,200 to 15,000 ohm-cm². The Inconel test length was 20 feet. From figure 20 this results in an input resistance of 3,000 ohms. For an open circuit potential difference of 0.25 volt (as initially observed), the predicted current would be in the range of 72 to 74 μ A. This is very close to the measured current about 1 hour after the initiation of testing. Higher corrosion rates would have been expected with longer lengths of either Inconel or 70/30 CuNi.

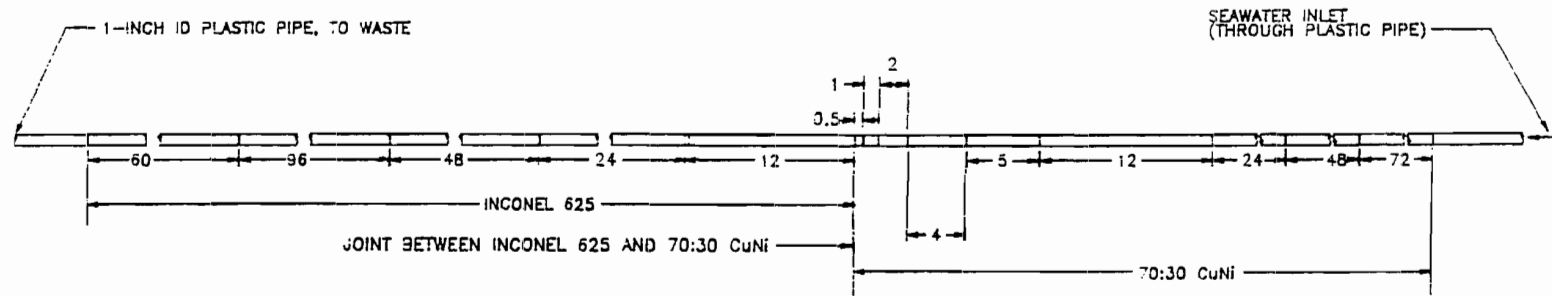
Conclusions

1. Pitting corrosion, the predominant form of corrosion for the alloy tested, does not necessarily follow the predicted attenuation as distance from the galvanic couple is increased. While the effects of the galvanic couple will attenuate with increasing distance, it is not unreasonable to expect that the maximum pitting rate will occur some distance from the actual couple. This precludes any meaningful life prediction from the mathematical model discussed in the *Introduction*.
2. Mathematical models can provide an estimate of the magnitude of galvanic current that would be expected to flow between segments of mixed metal seawater piping systems. These models can also suggest the extent or length of piping over which this current would attenuate.
3. The accuracy of these models is only as good as the data input to the models -- if the data input is not representative of the current electrochemical conditions, the model output is faulty. The present simple laboratory tests have shown that the electrochemical parameters can vary significantly during the lifetime of a structure. This also precludes meaningful life prediction from mathematical models.
4. The models are limited by their inability to accurately model the effects of current density on polarization resistance and the effect of time on polarization resistance. Also very important is the variation in EMF along the anodic or cathodic half-cell over time and distance from the couple. The current testing has shown that the EMF can vary over time and that it can vary along the length of each half-cell.
5. Given the variation in actual electrochemical parameters, the output of any model should be reviewed carefully. Extreme sophistication in computational effort does not necessarily insure results any more meaningful than those that might be provided by much simpler models. Truly accurate models must consider time effects that can be chaotic, and thus very difficult, if not impossible, to quantify. Often simple estimates are as accurate and meaningful as complex analysis.



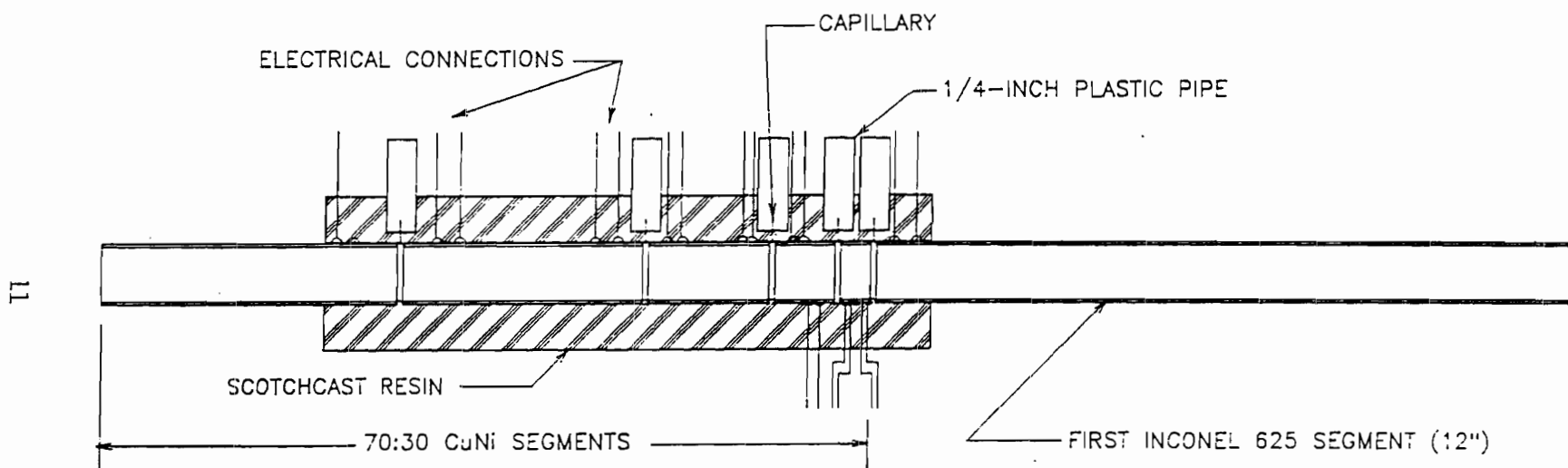
GENERAL ARRANGEMENT GALVANIC COUPLE TESTING

Figure 1



GENERAL ARRANGEMENT
GALVANIC COUPLE TEST PIPING

Figure 2



SEGMENT ASSEMBLY METHOD

Figure 3

INCONEL 625-70/30 CuNi COUPLE

MAXIMUM PIT DEPTHS

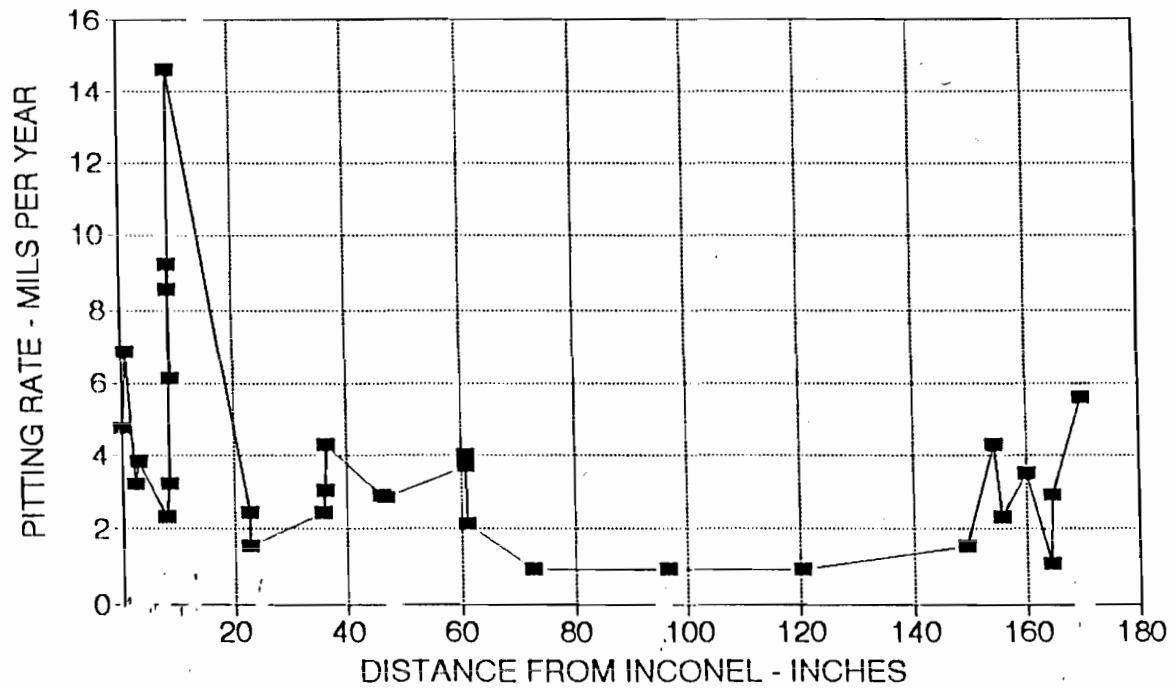


Figure 4

Figure 5. Internal Surface of 70/30 CuNi Tubing Nearest
the Inconel 625 (20X magnification).

INCONEL 625 - 70:30 CuNi COUPLE

TOTAL GALVANIC CURRENT AT START-UP

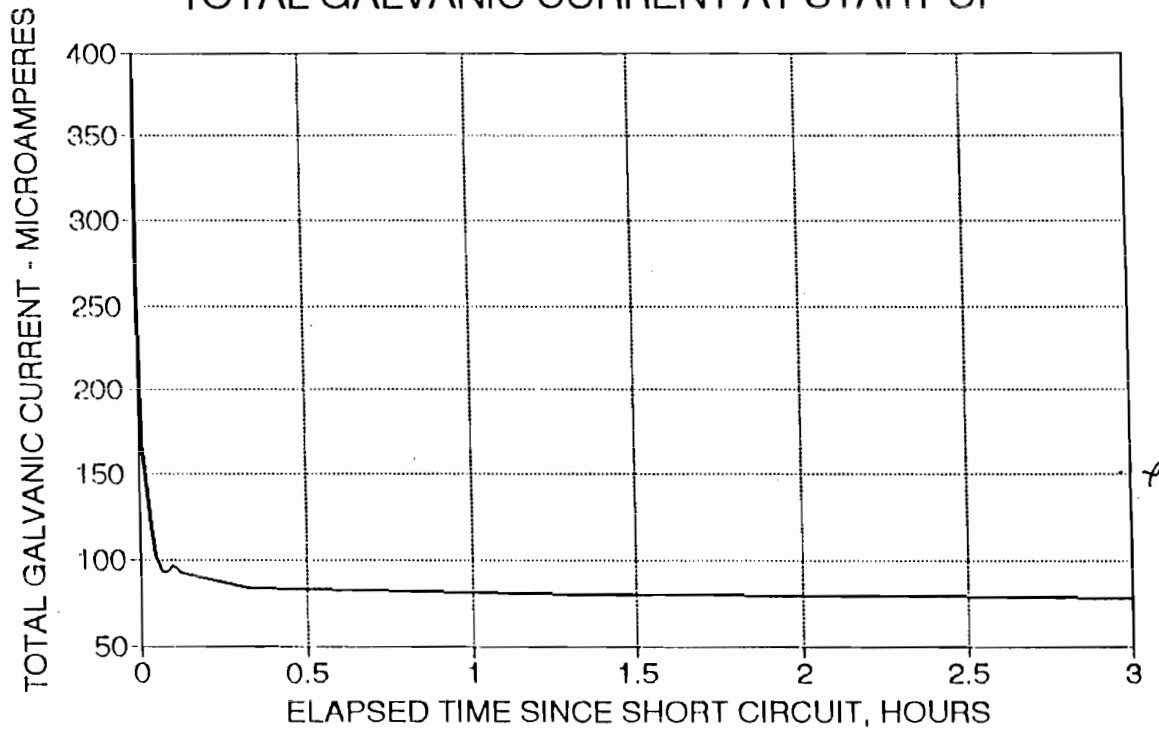


Figure 6

INCONEL 625/70-30 CuNi COUPLE
OPEN CIRCUIT POTENTIALS, 1/27/92

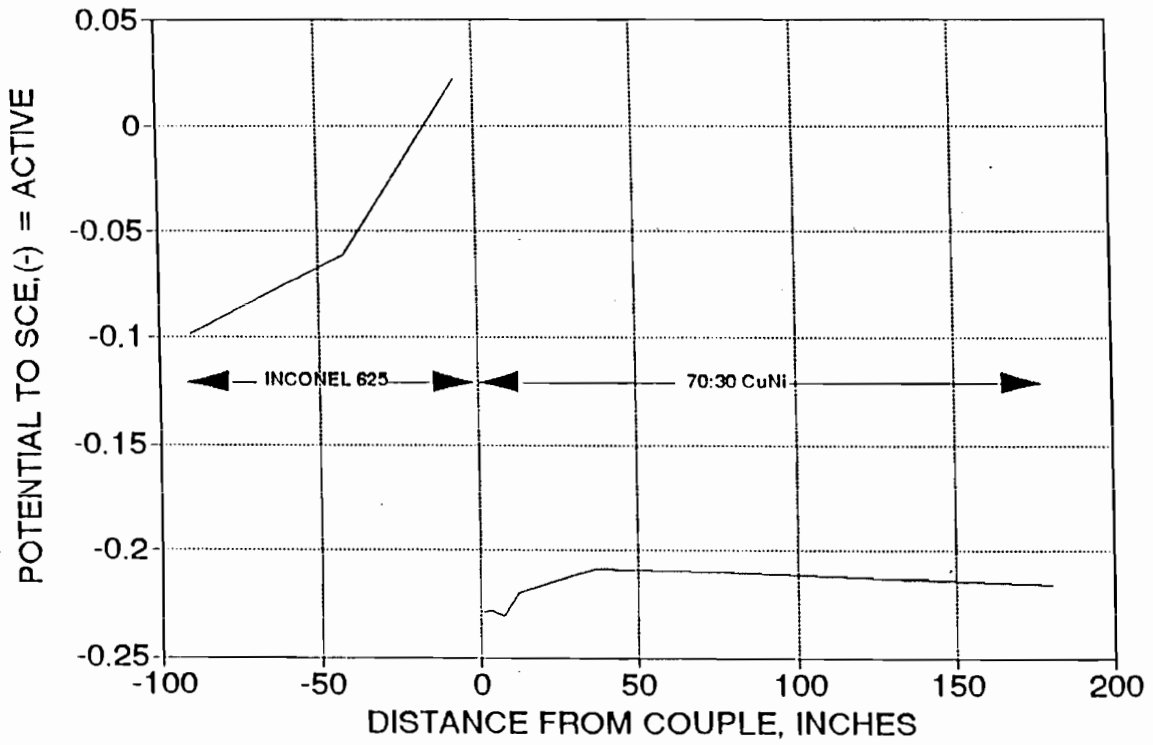


Figure 7

INCONEL 625 - 70:30 CuNi COUPLE

TOTAL GALVANIC CURRENT AT START-UP

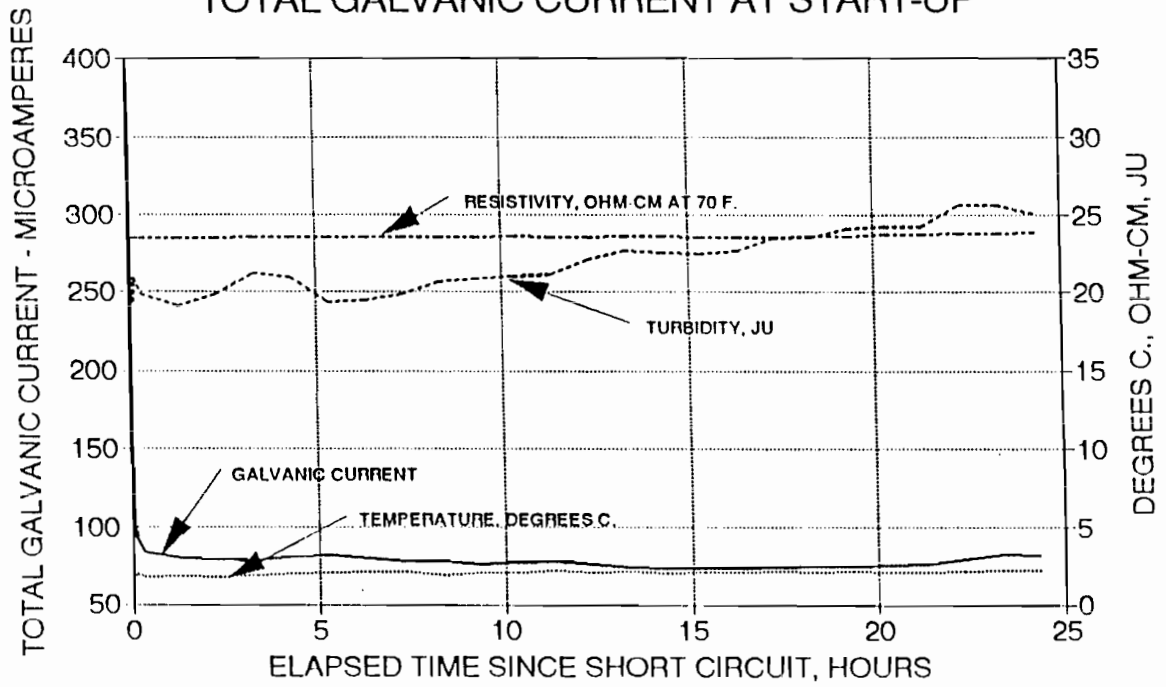


Figure 8

INCONEL 625 - 70:30 CuNi COUPLE POTENTIAL PROFILE

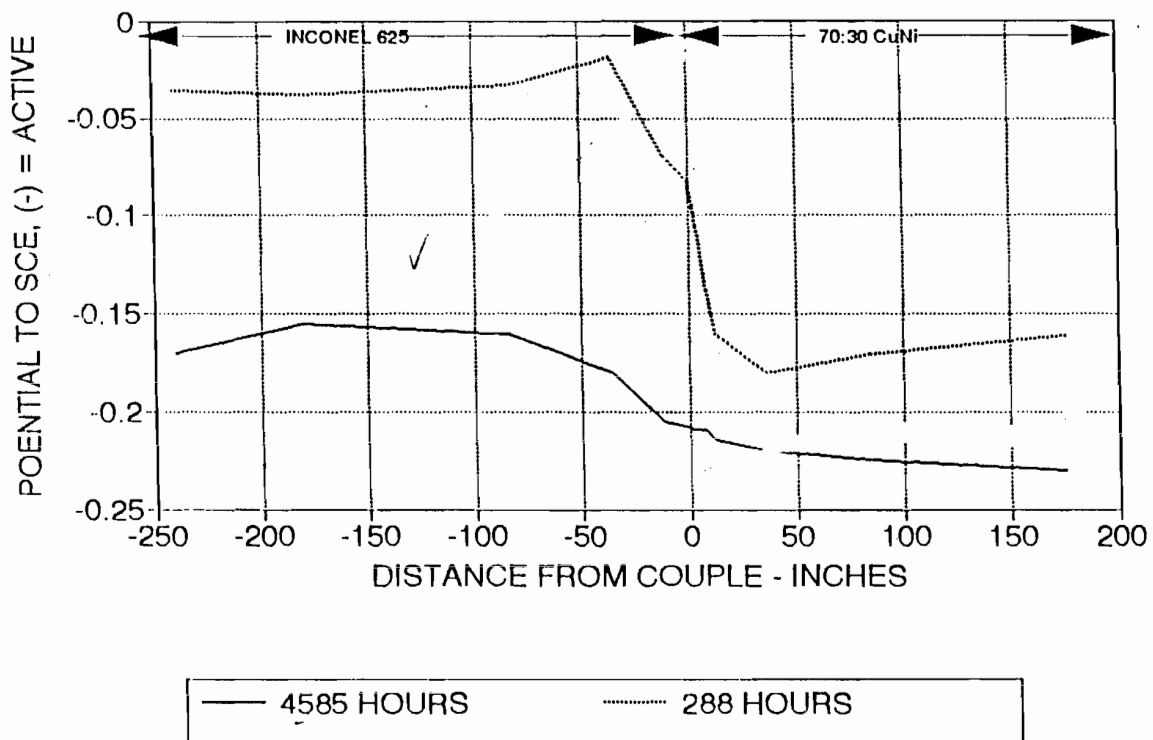


Figure 9

INCONEL 625-70/30 CuNi COUPLE
CURRENT PROFILES AT FOUR PERIODS

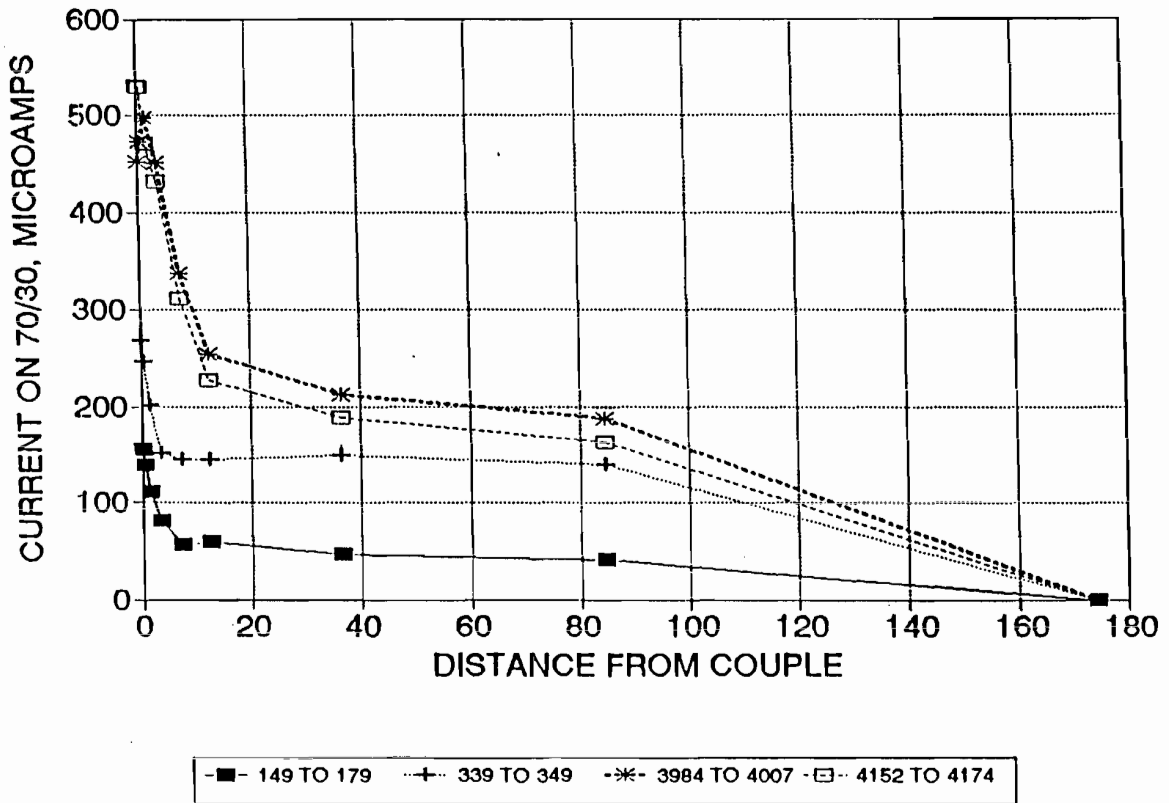


Figure 10

RESISTIVITY VS. TEMPERATURE

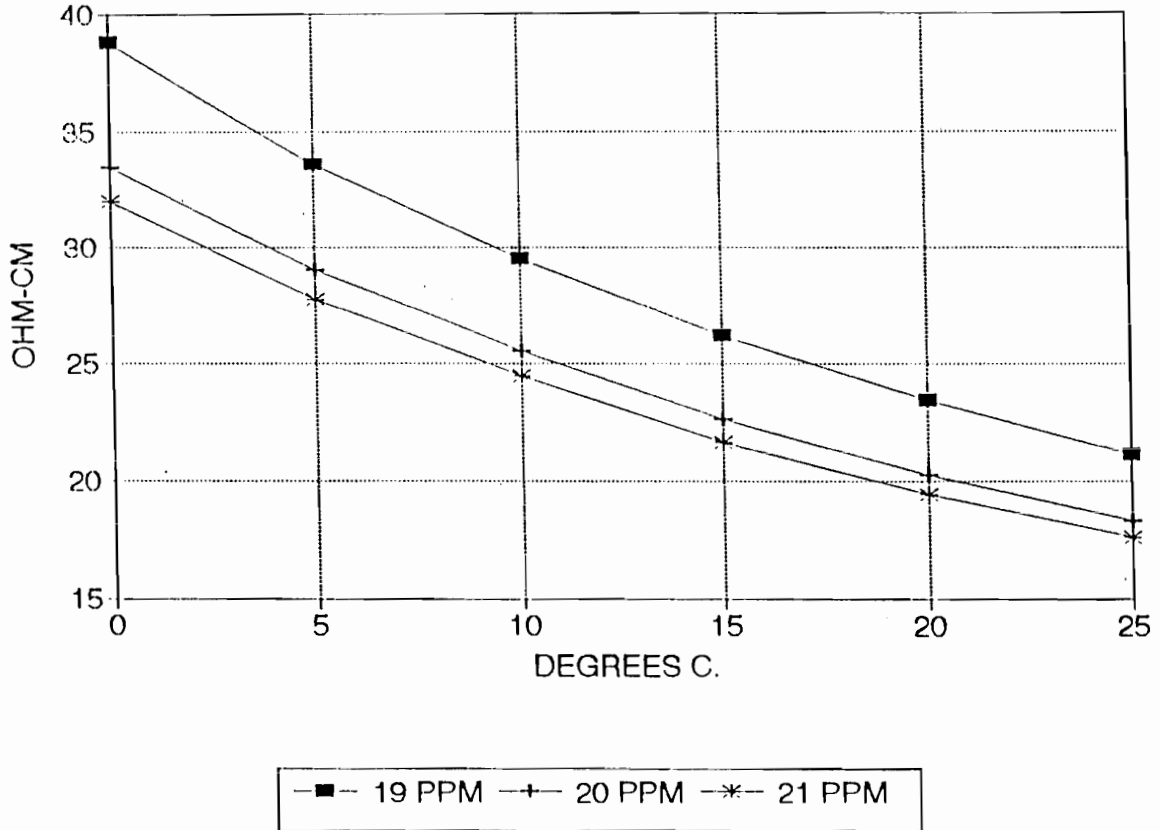


Figure 11

INCONEL 625 - 70:30 CuNi COUPLE

CURRENT INTERCHANGE DENSITY

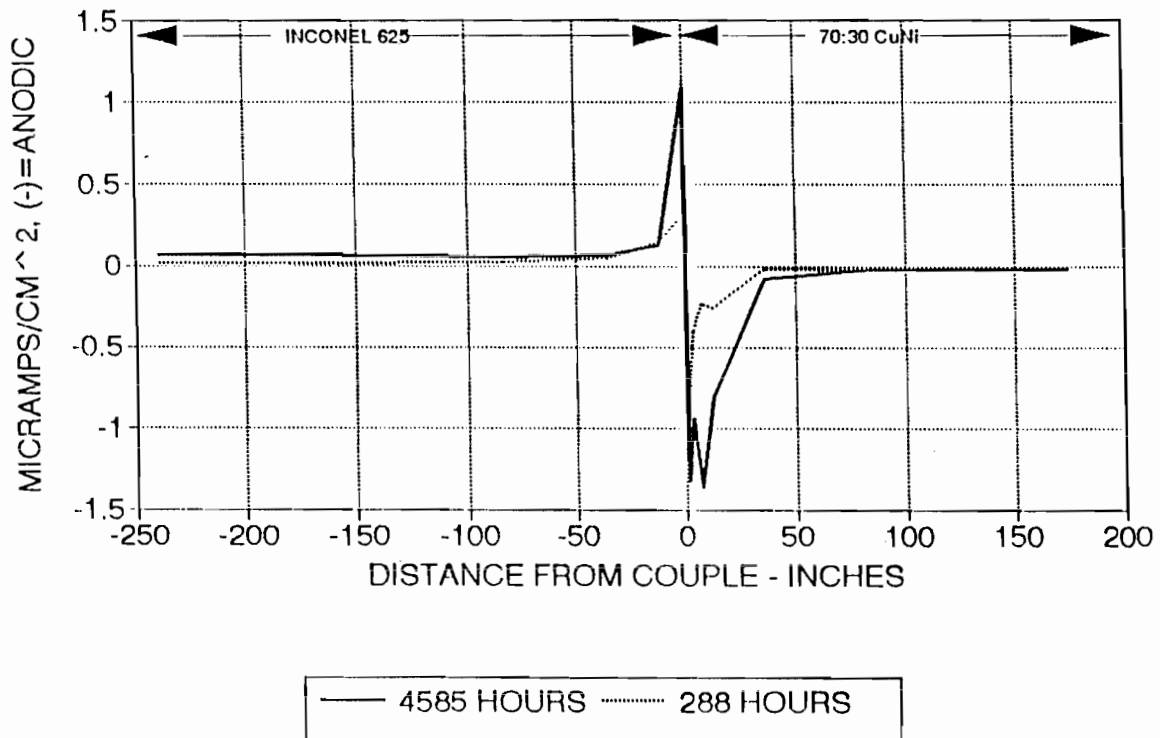


Figure 12

INCONEL 625, 70/30 CuNi COUPLE

2000 TO 2020 HOURS

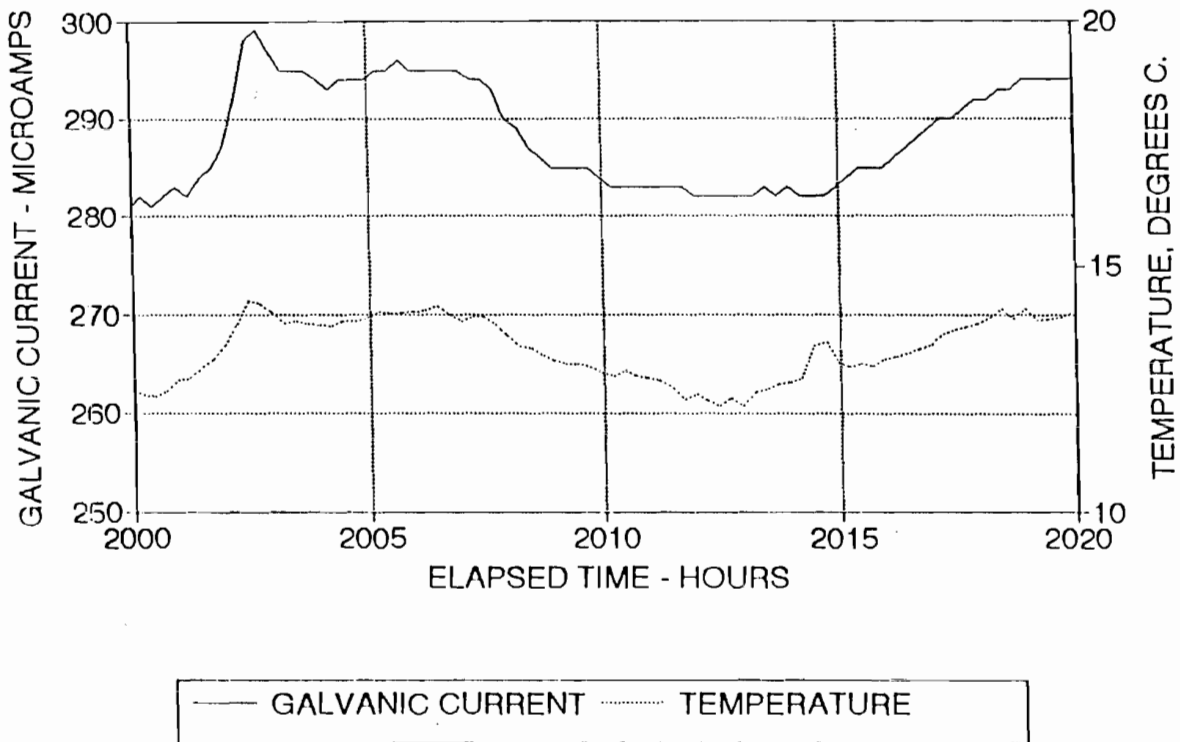


Figure 13

INCONEL 625 - 70/30 CuNi COUPLE

GALVANIC CURRENT, 4150 TO 4173 HOURS

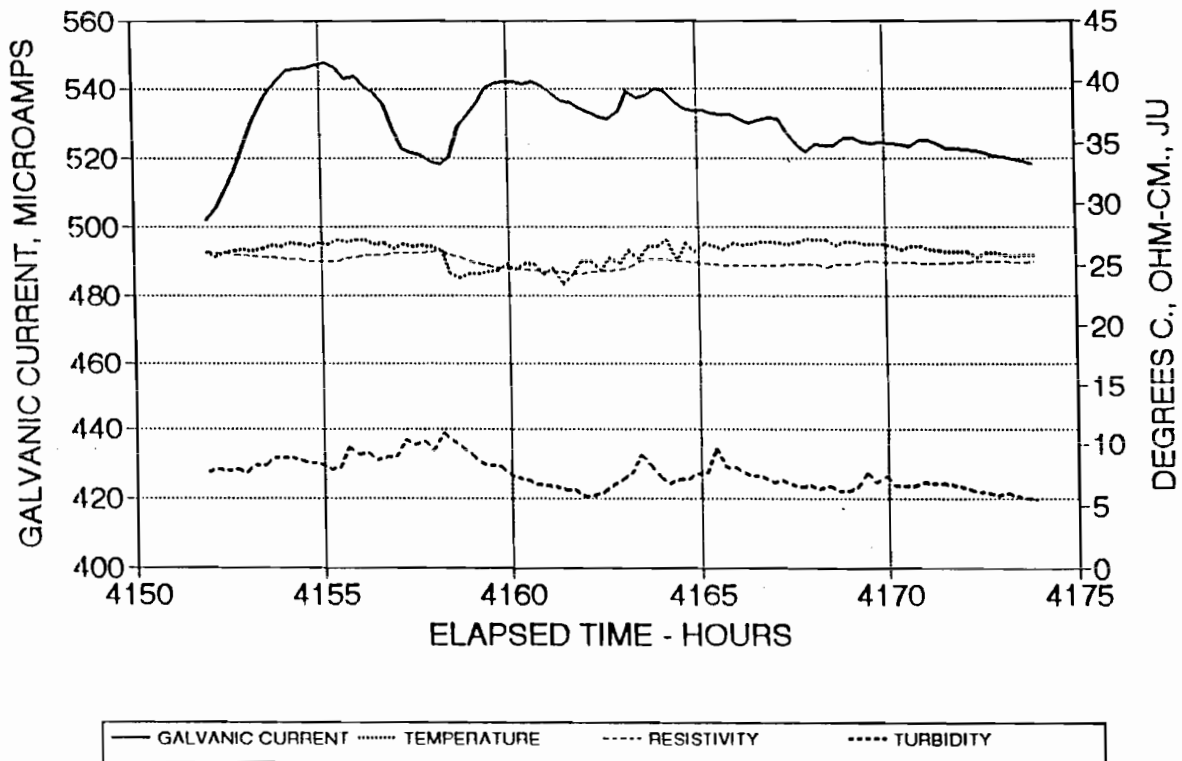


Figure 14

INCONEL 625 - 70:30 CuNi COUPLE

70:30 CuNi ANODIC POLARIZATION

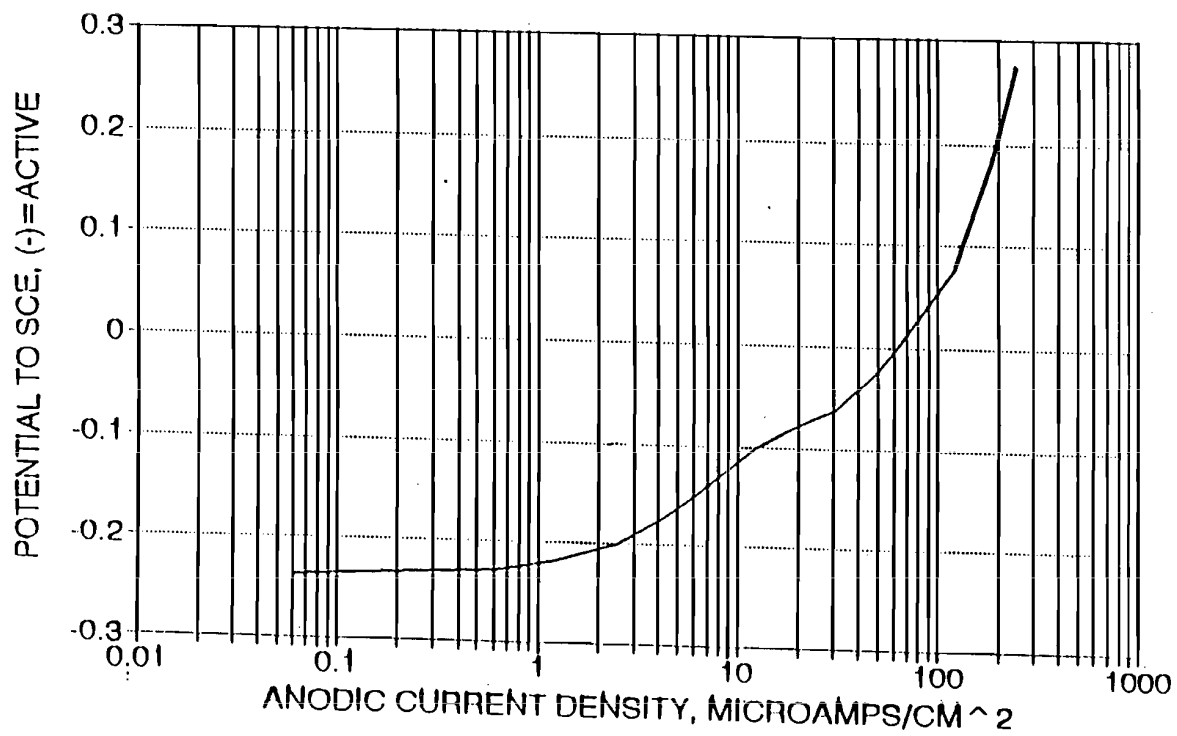


Figure 15

INCONEL 625 - 70:30 CuNi COUPLE

70:30 CuNi ANODIC POLARIZATION

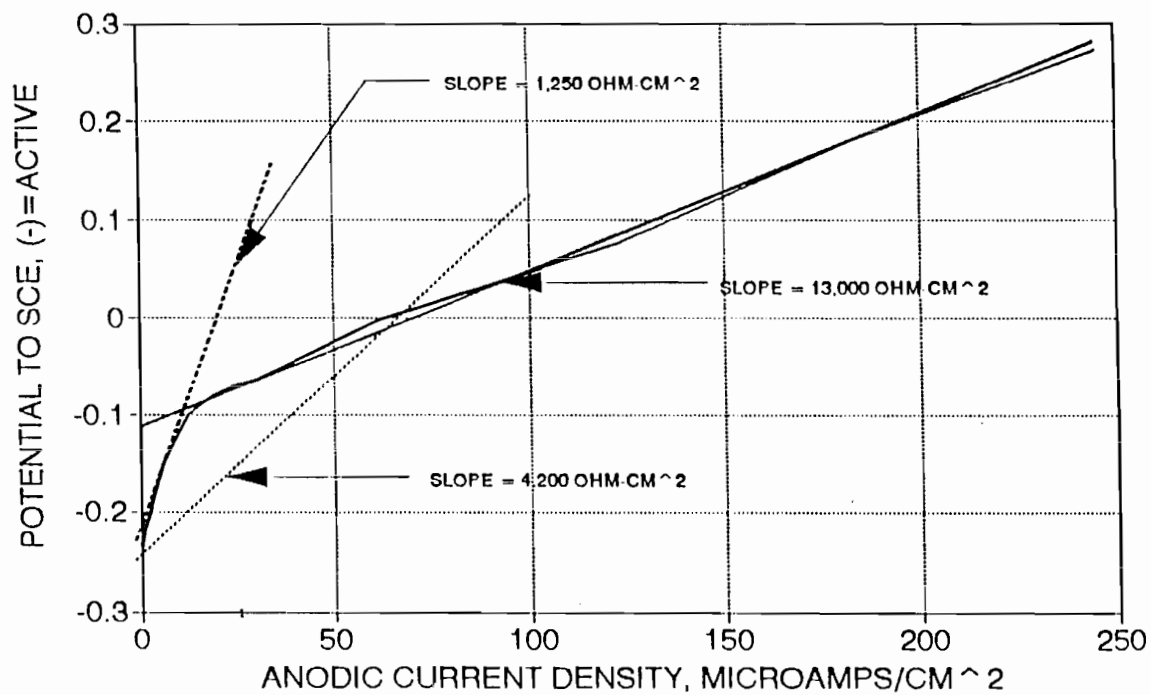


Figure 16

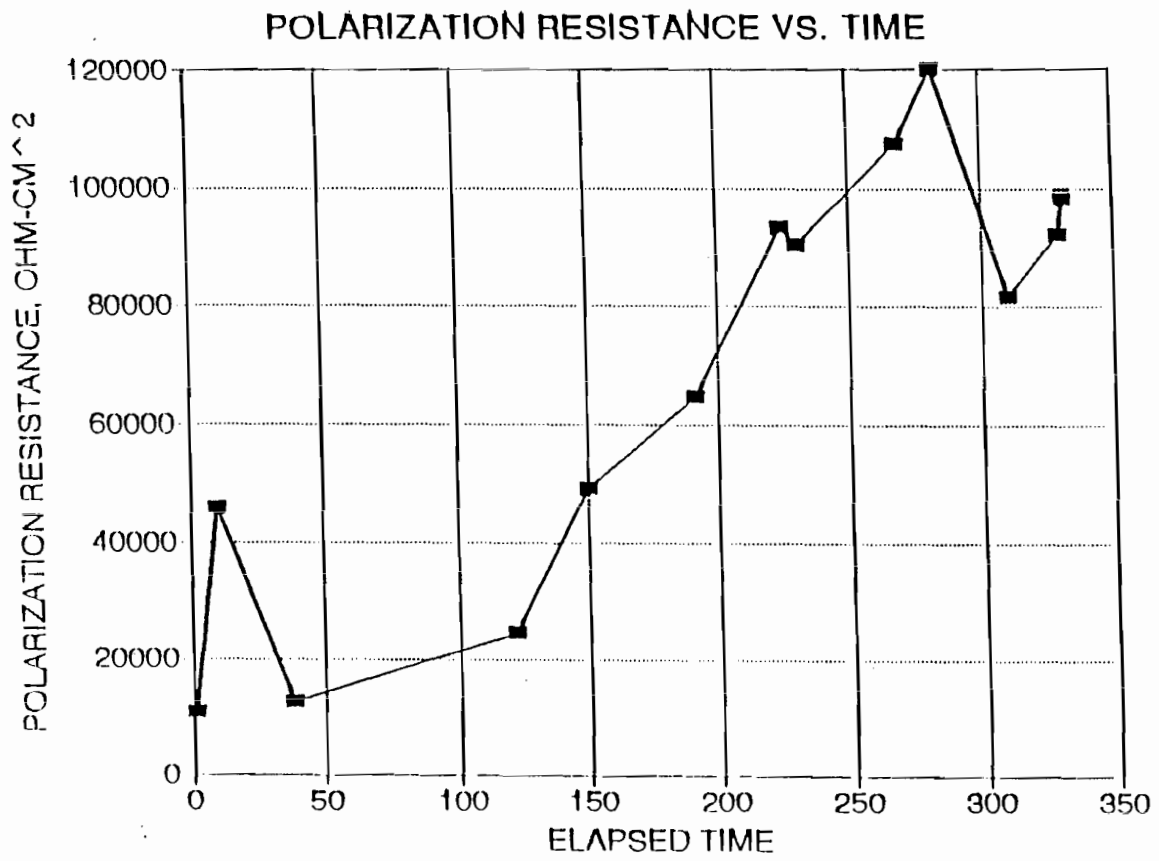
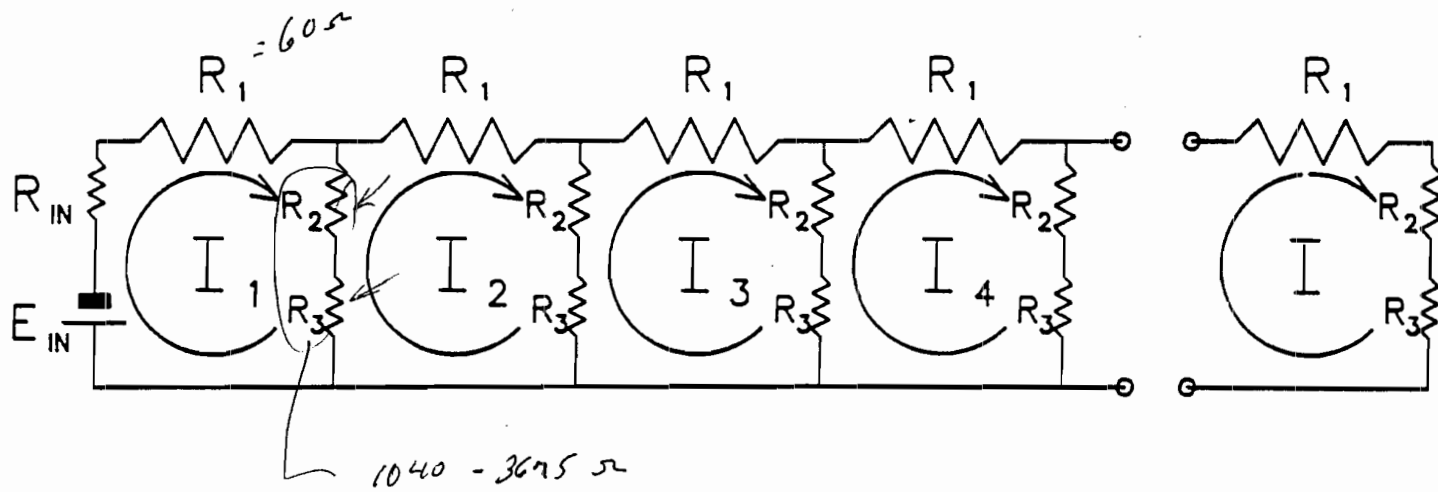


Figure 17



TEE SECTION EQUIVALENT CIRCUIT

Figure 18

INCONEL 625 - 70:30 CuNi COUPLE POLARIZATION EFFECTS

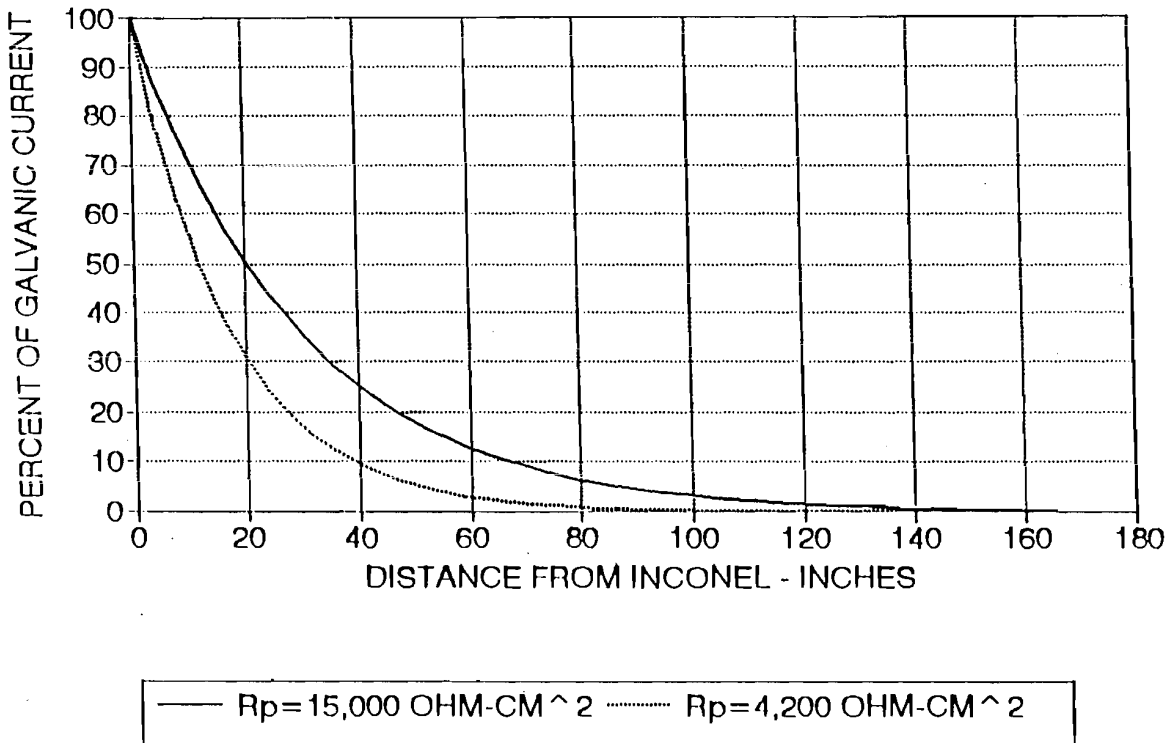


Figure 19

INCONEL 625 - 70:30 COUPLE

INPUT RESISTANCE - INCONEL 625

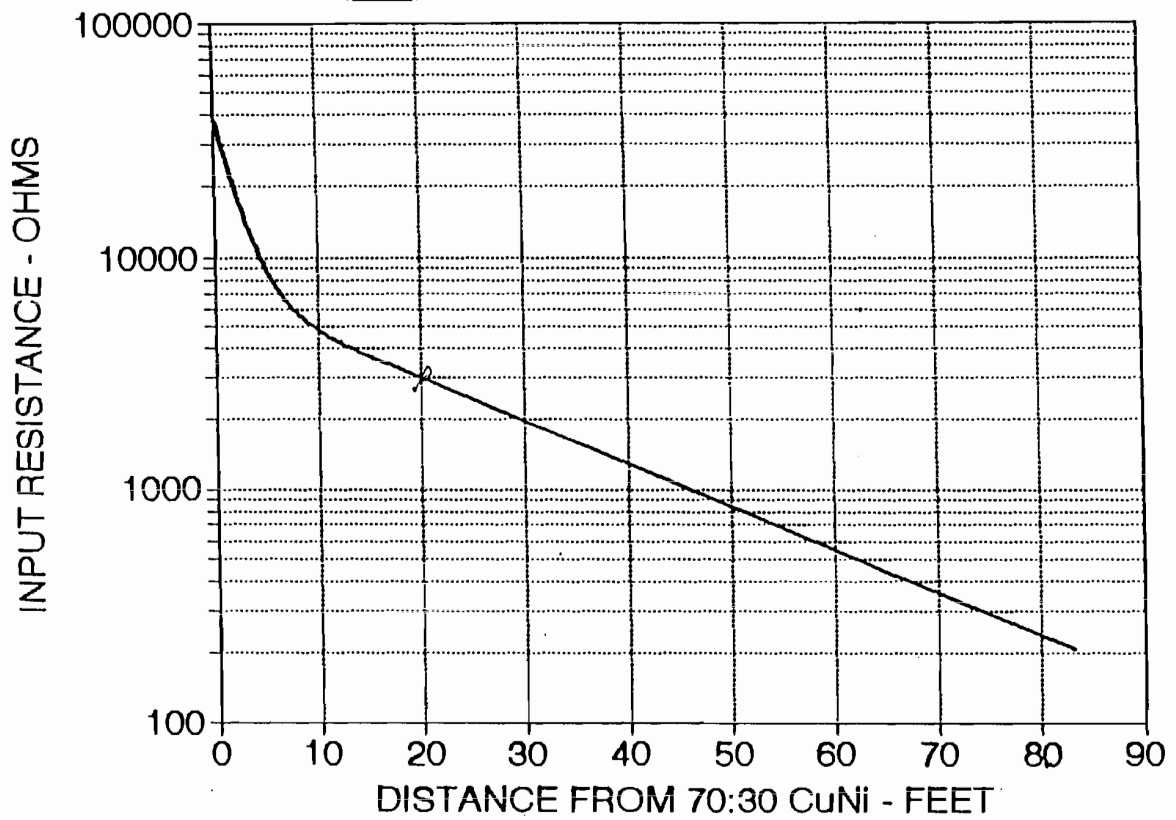


Figure 20